

Confinement transition of \mathbb{Z}_2 gauge theories coupled to massless fermions: emergent QCD_3 and $SO(5)$ symmetry

Snir Gazit,¹ Fakher F. Assaad,² Subir Sachdev,^{3,4} Ashvin Vishwanath,³ and Chong Wang³

¹*Department of Physics, University of California, Berkeley, CA 94720, USA*

²*Institut für Theoretische Physik und Astrophysik,
Universität Würzburg, 97074 Würzburg, Germany*

³*Department of Physics, Harvard University, Cambridge MA 02138, USA*

⁴*Perimeter Institute for Theoretical Physics,
Waterloo, Ontario, Canada N2L 2Y5*

(Dated: June 5, 2018)

Abstract

We study a model of fermions on the square lattice at half-filling coupled to an Ising gauge theory, that was recently shown in Monte Carlo simulations to exhibit \mathbb{Z}_2 topological order and massless Dirac fermion excitations. On tuning parameters, a confining phase with broken symmetry (an antiferromagnet in one choice of Hamiltonian) was also established, and the transition between these phases was found to be continuous, with co-incident onset of symmetry breaking and confinement. While the confinement transition in pure gauge theories is well understood in terms of condensing magnetic flux excitations, the same transition in the presence of gapless fermions is a challenging problem owing to the statistical interactions between fermions and the condensing flux excitations. The conventional scenario then proceeds via a two step transition, involving a symmetry breaking transition leading to gapped fermions followed by confinement. In contrast, here, using large scale quantum Monte Carlo simulations, we provide further evidence for a direct, continuous transition and also find numerical evidence for an enlarged $SO(5)$ symmetry rotating between antiferromagnetism and valence bond solid orders proximate to criticality. Guided by our numerical finding, we develop a field theory description of the direct transition involving an emergent non-abelian ($SU(2)$) gauge theory and a matrix Higgs field. We contrast our results with the conventional Gross–Neveu–Yukawa transition.

I. INTRODUCTION

Classical and quantum phase transitions have traditionally been studied in the framework of the Landau-Ginzburg-Wilson paradigm. Phases are distinguished on the basis of whether they preserve or break global symmetries of the Hamiltonian. Two distinct phases can be separated by a continuous phase transition only when one of them breaks a single symmetry which is preserved in the other.

More recently, studies of correlated quantum systems have led to many examples of important physical models displaying phase transitions which do not fit this familiar paradigm. We can have continuous quantum phase transitions between phases which break distinct symmetries [1]. And upon allowing for topological order, several new types of quantum phase transitions become possible. We can have continuous phase transitions between a phase with topological order to a phase without topological order, both of which preserve all symmetries: the earliest example of this is the phase transition in the Ising gauge theory in 2+1 dimensions described by Wegner [2]. We can also have continuous quantum transitions between phases with distinct types of topological order, and many examples are known in fractional quantum Hall systems [3, 4]. We can have a continuous transition from a phase with topological order to one with a broken symmetry [5–7]. Finally, we can have phase transitions between a Dirac semimetal and various gapped states, including a symmetric gapped state without topological order dubbed symmetric mass generation [8–13]

Theories of these novel transitions all involve quantum field theories with deconfined emergent gauge fields. The presence of the gauge fields reflects the long-range quantum entanglement near the critical point: this entanglement is not easily captured by the symmetry-breaking degrees of freedom, or their fluctuations. The gauge theories have varieties of Higgs and confining phases, and transitions between these phases allow for the transitions described above.

In the present paper, we will present a novel example of a deconfined critical point, between a deconfined phase with topological order and a confining phase with broken symmetry. The deconfined phase has Z_2 topological order, but in contrast to conventional topologically ordered states which are gapped, it also features gapless fermionic excitations, whose gaplessness is protected by the symmetries of the underlying Hamiltonian. This is an example of a ‘nodal’ Z_2 topological order, that has been invoked in the context of the square lattice antiferromagnet [14], and in the Kitaev model on the honeycomb lattice [15]. Here, we will augment the model to include both spin and charge conservation leading to a larger number of Dirac fermions (four flavors of complex two component fields) which can be simulated without a sign problem. Thus, we will be studying how the confinement transition in a gauge theory is modified by the presence of gapless charged fermions.

The confining phase, in the formulation used in our paper, is an insulator on the square lattice at half-filling with two-sublattice antiferromagnetic (AFM) order, similar to that found in a cuprate compound like La_2CuO_4 . The topologically ordered phase is also at half-filling. This phase can be considered as a toy model of a ‘pseudogap’ phase relevant to the doped cuprate superconductors, although our analysis will be restricted to half-filling. We will argue that there is a direct transition between the insulating antiferromagnet and the phase with topological order, and present a critical field theory with an emergent non-abelian $SU(2)$ gauge field.

Emergent symmetries will also play an important role in the analysis of our deconfined critical point. These are symmetries which are not present in the underlying Hamiltonian, or in the non-critical phases, but which become asymptotically exact at long distances and times in the critical regime. An emergent $SO(5)$ symmetry was proposed [16–18] for the deconfined critical point between the insulating AFM and valence bond solid (VBS) states on the square lattice: numerical computations on lattice models have observed such enhanced symmetries [19–23]. We will present numerical evidence for the same $SO(5)$ symmetry between the AFM and VBS order parameters in our model. This emergent symmetry is intriguing, because neither of the two phases near the transition (OSM or AFM) involves actual long-range VBS order, and yet VBS fluctuations become as strong as AFM fluctuations at the critical point. As we shall see later, this feature arises naturally in our formulation of the critical theory.

We shall study a model introduced in recent quantum Monte Carlo (QMC) studies [24, 25]. The model can be considered as an effective theory of electrons (c) on the square lattice. The model is expressed as an Ising lattice gauge theory (ILGT) coupled to ‘orthogonal’ fermions (f). The QMC studies showed that this model exhibits a topological ordered ‘orthogonal semi-metal’ (OSM) phase: this phase has a \mathbb{Z}_2 topological order, and massless Dirac fermion excitations which carry \mathbb{Z}_2 electric charges and also the spin and electromagnetic charges of the underlying electrons (c). The charges carried by these fermions are identical to the ‘orthogonal fermions’ introduced in Ref. [26], and so we have adopted their terminology. The previous studies also presented evidence for a confining AFM phase, along with a possible direct and continuous phase transition between the OSM and AFM phases. However the underlying mechanism of this transition was not understood.

Our QMC simulation finds numerical evidence for an emergent $SO(5)$ symmetry, rotating between AFM and VBS orders, at criticality. We contrast this finding with the more standard Gross–Neveu–Yukawa (GNY) universality class, where such an enlarged symmetry is absent. Guided by the numerical results, we conjecture that the critical theory describing the confinement transition is given by a two-color ($SU(2)$) quantum chromodynamics (QCD) with $N_f = 2$ flavors of Dirac fermions coupled to a near critical matrix Higgs field. The Higgs mechanism is shown to naturally allow access to both the confined and deconfined phases, using a single tuning parameter. The

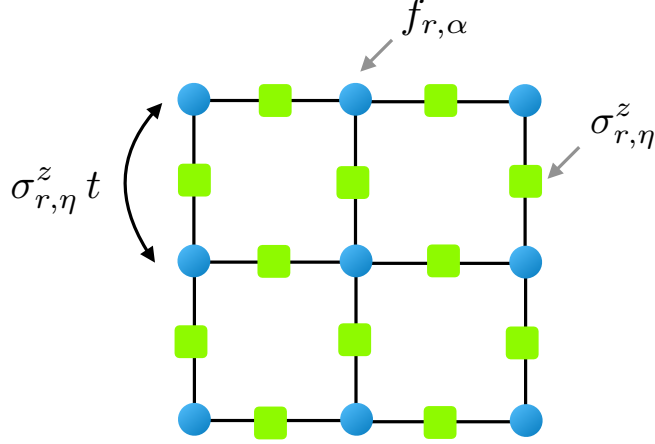


FIG. 1: Lattice model – the fermions $f_{r,\alpha}$ reside on the square lattice sites (blue circles) and the Ising gauge fields, $\sigma_{r,\eta}^z$ reside on the bonds (green squares). The Ising gauge field determines the sign of the hopping amplitude along the corresponding bond.

mechanism described here resembles the theory of symmetric mass generation (SMG) [12, 13] in some respects, but differs in the representation of the Higgs field under the gauge group. While SMG required Higgs fields transforming in the fundamental representation, so the Higgs phase was free of topological order, here we will employ a Higgs field in the adjoint representation, and the Higgs phase will therefore inherit a \mathbb{Z}_2 topological order along with gapless fermions.

II. MODEL, SYMMETRIES AND PHASE DIAGRAM

A. Model

We consider the Hamiltonian $\mathcal{H} = \mathcal{H}_{\mathbb{Z}_2} + \mathcal{H}_f$, illustrated in Fig. 1. The ILGT part of the Hamiltonian [2] reads,

$$\mathcal{H}_{\mathbb{Z}_2} = -J \sum_{\square} \prod_{b \in \square} \sigma_b^z - h \sum_b \sigma_b^x. \quad (2.1)$$

Here, σ_b^z and σ_b^x are the conventional Pauli matrices, \square labels the square lattice elementary plaquettes and $b = \{r, \hat{\eta}\}$ denotes the square lattice bonds with $r = \{r_x, r_y\}$ being the lattice site and $\hat{\eta} = \hat{x}/\hat{y}$. The fermionic part of the Hamiltonian is given by,

$$\mathcal{H}_f = -t \sum_{r, \hat{\eta}, \alpha} \sigma_{r, \hat{\eta}}^z f_{r+\hat{\eta}, \alpha}^\dagger f_{r, \alpha} + \text{h.c.} + U \sum_r \left(n_r^\uparrow - \frac{1}{2} \right) \left(n_r^\downarrow - \frac{1}{2} \right), \quad (2.2)$$

where, the operator $f_{r, \alpha}^\dagger$ creates an ‘orthogonal fermion’ [26] at site r with spin polarization α and $n_r = \sum_{\alpha} f_{r, \alpha}^\dagger f_{r, \alpha} = n_r^\uparrow + n_r^\downarrow$ is the fermion density.

By itself, this model cannot be a complete representation of the spin and charge excitations of a lattice electron model, like the Hubbard model. This is because it is not possible to write down a gauge-invariant electron operator, c_r , in terms of the f_r and the $\sigma_{r,\hat{\eta}}$. We need another bosonic degree of freedom which carries a \mathbb{Z}_2 electric charge. We will introduce such a degree of freedom later in the Section IV C; but for now, we assume that this boson is gapped in all the phases we study below, and we will not include it in our numerical study of \mathcal{H} .

As we demonstrate below, by varying the strength of the on-site Hubbard interaction term, in Eq. 2.2, we map a more generic phase diagram, compared to the ones obtained in Refs. [24, 25]. Furthermore, this extension allows us to test the stability of the OSM confinement transition, and to compare its critical properties with the more standard GNY and three dimensional classical Ising universality classes.

B. Symmetries

The global and local symmetries of the Hamiltonian will play an important role in our analysis. First, the Hamiltonian is invariant under global $SU_s(2)$ rotations corresponding to spin rotation symmetry. Second, because we restrict ourselves to half-filling, our model is also invariant under the particle-hole (PH) transformation $f_\alpha \rightarrow (-1)^{r_x+r_y} f_\alpha^\dagger$. Finally, combining PH symmetry with the $U_c(1)$ symmetry corresponding to particle number conservation forms an enlarged $SU_c(2)$ pseudo-spin symmetry rotating between charge density wave (CDW) and superconducting order parameters [27].

Partial particle-hole (PH) symmetry, acting only on one of the spin species, maps between the charge, n_r , and the spin, $S_r^z = n_r^\uparrow - n_r^\downarrow$, operators. Consequently, partial PH symmetry interchanges between the symmetries $SU_s(2)$ and $SU_c(2)$ and, when these symmetries are broken, between AFM and BCS/CDW orders respectively. The Hubbard term in Eq. (2.2) explicitly breaks partial PH symmetry, since under the symmetry action repulsive interaction is mapped to attractive interaction, $U \rightarrow -U$ [28].

The correspondence of our model to lattice gauge theories (LGT) is manifest in the extensive number of *local* Ising symmetries generated by the operators $G_r = (-1)^{n_r} \prod_{b \in +_r} \sigma_b^x$, with $+_r$ denoting the set of bonds emanating from the site r . The eigenvalues, $Q_r = \pm 1$, of G_r are conserved quantities and within the Hamiltonian formalism of LGT [29] are identified with the *static* background \mathbb{Z}_2 charge.

The Hilbert space then decomposes into a direct sum of subspaces labeled by the \mathbb{Z}_2 charge configuration Q_r , and comprises quantum states that obey an Ising variant of Gauss' law $G_r = Q_r$. For a uniform charge configuration, we can distinguish between two possibilities: an even LGT, $Q = 1$, with no background charge and an odd LGT, $Q = -1$ with a single \mathbb{Z}_2 background charge

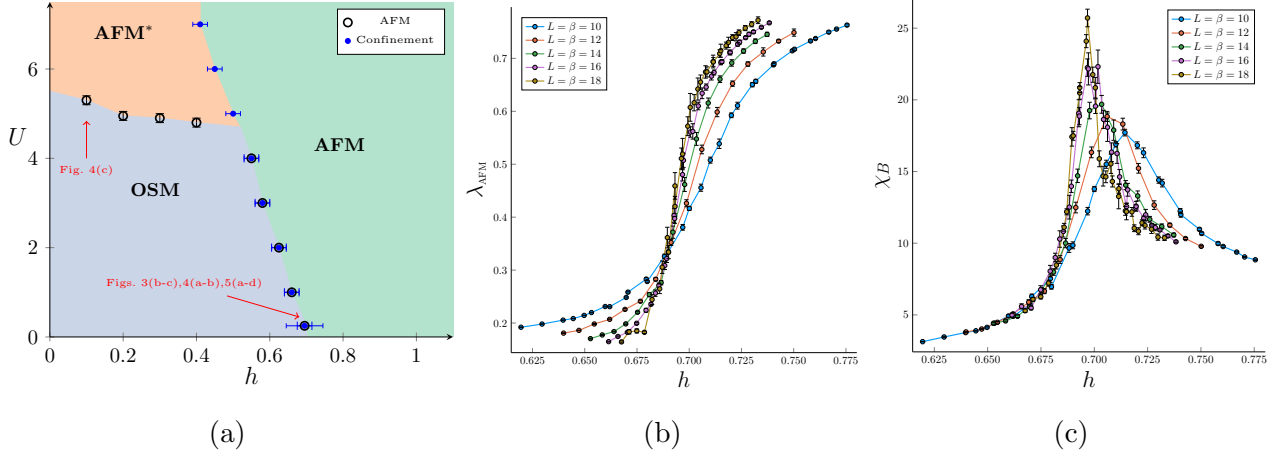


FIG. 2: (a) Phase diagram of the ILGT coupled to fermions. Red arrows point to parameter cuts studied in the figures below. (b-c) Simulation of the OSM confinement transition, carried out at $U = 0.25$ as a function of h . (b) The onset of AFM order is located by a curve crossing analysis of the susceptibility ratio λ_{AFM} and (c) the confinement transition is located from the divergence of the Ising flux susceptibility, χ_B .

at each site. We note that partial PH symmetry maps $Q \rightarrow -Q$.

Gauss's law can be either explicitly enforced [25], or alternatively, it is generated dynamically at sufficiently low temperatures [24]. In the numerical computation below, we will consider both options depending on numerical convenience. The zero temperature universal properties of our model, which are the focus of this study, do not depend on the above choice.

C. Phase diagram

We now determine the general structure of the zero temperature phase diagram (see Fig. 2a) by studying several limiting cases. For concreteness, we consider negative values of J (the case $J > 0$ is discussed in Ref. [25]) and set $-t = |J|$. All other energy scales are measured in units of $|J|$. We will only consider the odd LGT case, which, as we explain in the following, is compatible with repulsive Hubbard interactions, $U > 0$. The corresponding results for the even LGT can be easily obtained by applying a partial PH transformation with the appropriate identification of symmetries and order parameters, as discussed above.

We first consider the strong coupling limit $h \gg t, U, |J|$. In the extreme limit $h \rightarrow \infty$, the ILGT ground state is given by the product state $|\Psi_{\text{conf}}^\sigma\rangle = \prod_b |\sigma_b^x = 1\rangle$, as follows directly from minimizing the transverse field term in Eq. (2.1). In the above limit, we can safely neglect quantum fluctuations and substitute $\sigma_b^x = 1$ in the Ising Gauss's law. This yields the relation $Q_r = (-1)^{n_r}$

such that the local fermion parity, $(-1)^{n_f}$, becomes a conserved quantity, identified with the background Ising charge, Q_r .

Following the standard LGT analysis [29], we now establish the effective interaction between a pair of Ising charge excitations in the strong coupling limit. To comply with Ising Gauss's law, a string of flipped Ising gauge field, $\sigma_b^x = -1$, must connect any pair of Ising charges. The energy cost associated with each spin flip is proportional to h , and thus the interaction potential grows linearly with the separation giving rise to confinement.

The repulsive Hubbard interaction favors single on-site occupancy and consequently gaps even parity (doublons and holons) states. The resulting low energy sector is an odd LGT with a emergent Gauss law constraint $G_r = -1$. This leaves the on-site fermion spin as the only remaining dynamical degree of freedom. Reintroducing quantum fluctuations, at large but finite transverse field h , allows for virtual hopping processes. Similarly to the super-exchange mechanism, such fluctuations induce an effective AFM Heisenberg interaction proportional to t^2/h . The zero temperature ground state will then spontaneously break the spin rotational symmetry, $SU_s(2)$, by forming a Néel AFM state.

Next, we examine the weak coupling limit $J \gg t, h, U$. Here, minimizing the Ising flux term in Eq. (2.1) (for negative J) realizes a uniform π -flux state, $|\Psi_{\text{de-conf}}^\sigma\rangle = \prod_{\square} |\Phi_{\square} = -1\rangle$, where $\Phi_{\square} = \prod_{b \in \square} \sigma_b^z$ is the Ising flux threading the elementary plaquette, \square . Crucially, the single-particle spectrum of the π -flux lattice hosts a pair of gapless Dirac fermions [30]. In the resulting phase, the matter fields are deconfined, since, in contrast to the confining phase, gauge field fluctuations mediate only short-range attractive interaction with a vanishing string tension. The deconfined phase hosts fractionalized excitations carrying long-range entanglement [31]. We note that a π -flux phase can be stabilized even if J is positive by taking the large hopping amplitude t limit [24, 25].

The gapless deconfined phase resembles the well-known gapless \mathbb{Z}_2 spin liquid, using the condensed matter theory (CMT) parlance [14, 32]. However, there is one crucial difference: in our case the fermionic matter fields carry in addition to the $SU(2)$ spin charge (similarly to conventional spinons) an $U(1)$ electromagnetic charge. This makes our model more closely related to an orthogonal-metal construction [26], where the fractionalization pattern involves decomposing the physical fermion into a product of a fermion carrying both spin and charge and an Ising spin. Both slave particles carry an Ising gauge charge. We, therefore, dub this phase by the name orthogonal semi-metal (OSM).

Due to the vanishing density of states at half-filling, the Dirac phase is stable against AFM order for weak Hubbard interactions, $U \ll t$. However, a transition to an AFM* phase is expected at sufficiently large coupling. Here, the asterisk expresses the fact that the gauge theory remains deconfined in the AFM* phase. This situation should be contrasted with the confined phase, where along with AFM symmetry breaking order, the gauge sector is confined.

D. Phase transitions

The different phases of our model are classified according to the presence or absence of topological order and conventional symmetry breaking AFM order. Thus, the associated phase transitions are expected to involve either confinement or symmetry breaking or both.

More specifically, the phase transition between the deconfined Dirac phase and the AFM* phase is solely marked by the rise of AFM order, while the Ising gauge field sector remains deconfined. Therefore, the transition belongs to the conventional chiral GNY universality class [33–36]. On the other hand, across the transition between the confined AFM and AFM* phases the gapped fermions are only spectators and the transition is signaled by the emergence of topological order in the AFM* phase. Thus, the phase transition corresponds to the standard confinement transition of the pure Ising gauge theory, which belongs to the three dimensional classical Ising model universality class (the spin-wave (Goldstone) modes are not expected to modify the universality class of this transition, as can be seen by the methods of Ref. [37]).

The most interesting phase transition, which is the subject of this study, is between the deconfined Dirac phase and the confined AFM. Previous numerical simulations [24, 25] and new results shown below have found evidence for a single and continuous phase transition involving both symmetry breaking and confinement. Gaining a better analytic and numerical understanding of this transition is the main subject of the remainder of this paper.

III. QUANTUM MONTE CARLO

A. Methods

The ILGT coupled to fermions is free of the numerical sign-problem for arbitrary fermion density (here we are interested only in the half-filled case) [24, 25]. This allows us to study our model using an unbiased and a numerically exact (up to statistical errors) QMC simulations. We employ the standard auxiliary-field QMC algorithm [38, 39] using both single spin-flip updates and global moves inspired by the worm algorithm [25]. In all cases, we set the imaginary time Trotter step to be $|t|\Delta\tau = 1/12$, a value for which the discretization errors are controlled. In what follows, we set $t = J = -1$ and explore the phase diagram as a function of h and U . Unless otherwise stated, we also explicitly impose Gauss’s law constraint. Further technical details of our numerical scheme as well as additional numerical data can be found in Appendices A, B and C.

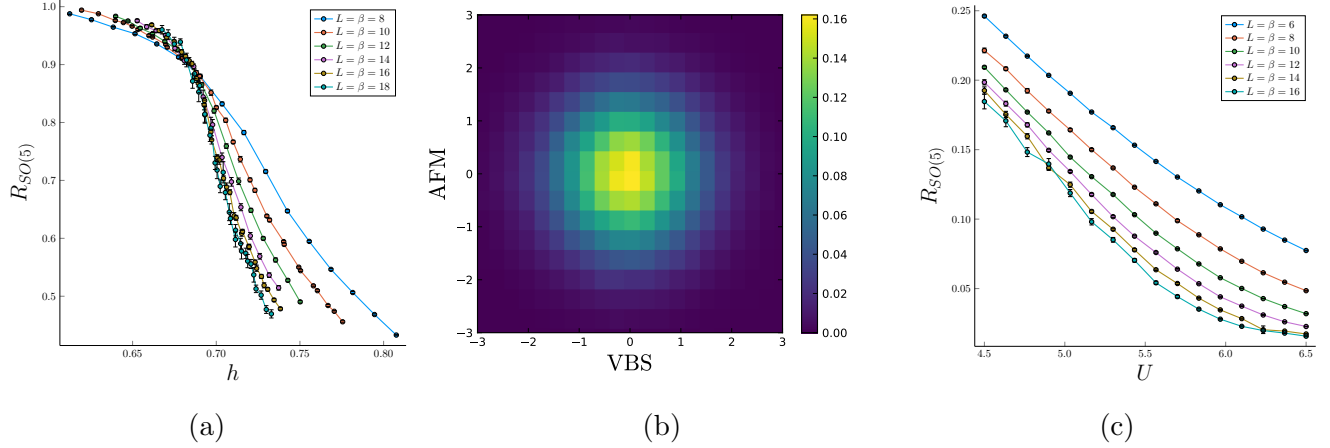


FIG. 3: Signature of an $SO(5)$ symmetry. (a) A clear curve crossing is observed in the susceptibility ratio $R_{SO(5)}$ across the OSM confinement transition for $U = 0.25$ as a function of h . (b) Joint probability distribution $\mathbf{P}(D^x, \mathbf{S}^z)$ of the VBS and AFM order parameters at criticality. $\mathbf{P}(D^x, \mathbf{S}^z)$ exhibits a circular symmetry (c) Susceptibility ratio $R_{SO(5)}$ across the AFM transition for $h = 0.1$ as a function of U . The absence of curves crossing rules out the emergence of an $SO(5)$ symmetry at the GNY transition.

B. Observables

We probe the VBS and AFM order parameters using the bond kinetic energy, $\mathbf{D}^{x/y}$, and the fermion spin, \mathbf{S}^γ , operators, respectively. Their corresponding lattice definitions at finite wave vector, q , are given by,

$$\begin{aligned} \mathbf{D}^\eta(q) &= \sum_{r,\alpha} e^{iq \cdot r} \left(\sigma_{r,\eta}^z f_{r+\eta,\alpha}^\dagger f_{r,\alpha} + \text{h.c.} \right) \\ \mathbf{S}^\gamma(q) &= \sum_{r,\alpha,\beta} e^{iq \cdot r} f_{r,\alpha}^\dagger \tau_{\alpha\beta}^\gamma f_{r,\beta} \end{aligned} \quad (3.1)$$

where, $\tau_{\alpha\beta}^\gamma$ are the usual Pauli matrices.

On the π -flux square lattice, the set of fermion bilinears appearing in Eq. 3.1 form a five component super-vector that transforms as a fundamental under $SO(5)$ rotations. Within this formalism, the competition between AFM and VBS fluctuations is explicitly manifest [16, 17].

To study fluctuations, we use the imaginary time static susceptibility, which for a generic operator, \mathcal{O} , is defined by $\chi_{\mathcal{O}}(q) = \frac{1}{\beta L^2} \left\langle \left(\int_0^\beta d\tau \mathcal{O}(q, \tau) \right)^2 \right\rangle$. Here, expectation values are defined with respect to the thermal density matrix, $\beta = 1/T$ is the inverse temperature T , and L is the linear system size. The ordering wave vector associated with AFM (VBS) order (along the \hat{x}/\hat{y} bonds) equals $G_{\text{AFM(VBS)}} = \{\pi, \pi\}(\{\pi, 0\}/\{0, \pi\})$.

To locate the onset of AFM order, we use the renormalization group (RG) invariant ratio

$\lambda_{\text{AFM}} = 1 - \chi_{\text{S}}(G_{\text{AFM}})/\chi_{\text{S}}(G_{\text{AFM}} - \Delta q)$, with $|\Delta q| = 2\pi/L$ being the smallest wave vector on our finite lattice. λ_{AFM} approaches unity deep in an AFM phase and vanishes when the symmetry is restored [40]. For a continuous transition, curves of λ_{AFM} corresponding to different Euclidean space-time volumes are expected to cross at the critical coupling. Anticipating the emergence of strong VBS fluctuations at criticality, we also define the analogous RG ratio, $\lambda_{\text{VBS}} = 1 - \chi_{\text{D}}(G_{\text{VBS}})/\chi_{\text{D}}(G_{\text{VBS}} - \Delta q)$.

For pure lattice gauge theories, it is standard to probe confinement via the Polyakov loop [41]. In the presence of matter fields, the Polyakov loop no longer sharply defines confinement due to charge screening. In principle, one can detect the rise of topological order by extracting the topological contribution to the entanglement entropy [42, 43] or by measuring the Fredenhagen-Marcu [44, 45] order parameter. However, such probes are difficult to reliably scale with system size in fermionic QMC simulations. In our analysis, we detect the thermodynamic singularity associated with the confinement transition by probing the expected divergence of the Ising flux susceptibility, $\chi_B = \partial\langle\Phi\rangle/\partial J$, with Φ being the Ising flux density defined above [25].

C. Numerical Results

Our first task is to determine numerically the phase diagram shown in Fig. 2a. We exemplify our analysis by studying the OSM confinement transition. For concreteness, we fix $U = 0.25$, and drive the transition by increasing the strength of the transverse field, h . In our finite size scaling analysis, we consider linear system sizes up to $L = 18$. We further assume relativistic scaling and accordingly consider inverse temperatures that grow linearly with the system size, $\beta = L$.

In Fig. 2b, we track the evolution of λ_{AFM} as a function of h . We observe a clear curve crossing that varies very little with system size and strongly indicates a continuous transition. The crossing point marks the rise of AFM order and allows us to estimate the critical coupling, $h_c^{\text{AFM}}(U = 0.25) = 0.69(2)$. Moving to the IGLT sector, in Fig. 2c, we depict the Ising flux susceptibility, χ_B , across the confinement transition. With increase in the system size, χ_B displays a progressively diverging and narrowing peak. We use the peak position to estimate the critical coupling of the confinement transition to be $h_c^{\text{conf}} = 0.69(2)$. This value coincides, within the error bars, with the emergence of AFM order, found above, suggesting that symmetry breaking and confinement occur simultaneously.

We employ a similar analysis to determine the rest of the phase boundaries appearing in Fig. 2a. We find that the critical confinement line separating the AFM and AFM* phases meets with the AFM transition line separating the OSM and the AFM* phases at a tricritical point. The two critical lines then merge into a single line corresponding to the OSM confinement transition.

We now test the emergence of enlarged symmetries in the OSM confinement transition. In the

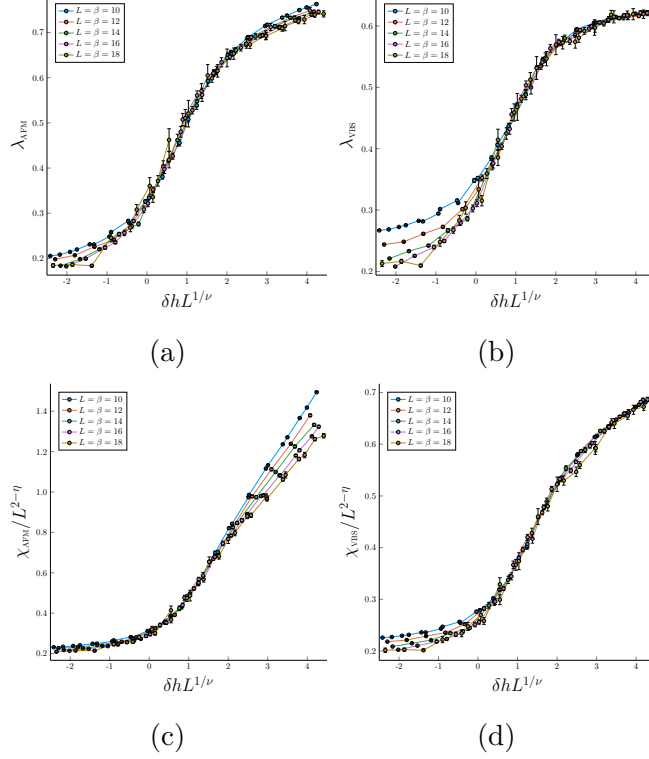


FIG. 4: Finite size scaling analysis of (a) λ_{AFM} (b) λ_{VBS} (c) χ_{AFM} and (d) χ_{VBS} . In all cases, curve collapse is obtained using the critical coupling $h_c = 0.69$, the correlation length exponent $\nu = 0.58$. The *same* anomalous exponent $\eta = 1.4$ is used to scale both the AFM and VBS fluctuations.

presence of an $SO(5)$ symmetry, the scaling dimension of the VBS and AFM order parameters must coincide [19]. As a direct consequence, similarly to λ_{AFM} , the susceptibilities ratio, $R_{SO(5)} = \chi_{\text{AFM}}(G_{\text{AFM}})/\chi_{\text{VBS}}(G_{\text{VBS}})$ becomes a renormalization group (RG) invariant.

In Fig. 3a, we depict the susceptibility ratio, $R_{SO(5)}$, as a function of h , across the confinement transition, for different system sizes. Indeed, we find that all curves cross at a single point, independent of the space-time volume. We use the crossing point to pin down the critical coupling, $h_c^{SO(5)} = 0.69(2)$, in excellent agreement with the above calculations, using other observables. We note that this result is a necessary but not a sufficient condition for the emergence of an $SO(5)$ symmetry. Nevertheless, it serves as a non-trivial test for this effect.

To further illustrate the emergence of an $SO(5)$ symmetry, in Fig. 3b, we depict a two dimensional histogram approximating the joint probability distribution of the VBS and AFM order parameters at criticality. We note that due to algorithmic limitations, in computing the AFM histogram, one must simulate the constraint-free model. Doing so, only slightly shifts the critical coupling and as explained above, it does not affect critical properties. Remarkably, the joint dis-

tribution exhibits a circular form, which provides further indication for the emergence of an $SO(5)$ symmetry. We have also verified, using a similar analysis, that the joint probability distribution of the VBS order along the x and y directions affords an emergent, $SO(2)$, rotational symmetry at criticality, see Appendix B.

To better appreciate the above result, it is instructive to apply the susceptibility ratios analysis on the more conventional GNY transition. To that end, we investigate the transition between the OSM phase and the AFM* phase. We fix $h = 0.1$, and cross the AFM transition by increasing U . The results of this analysis are shown in Fig. 3c. In stark contrast to the confinement transition, we find no evidence for a curve crossing. Thus, we can deduce that the putatively continuous OSM confinement transition must belong to a universality class that is *distinct* from the conventional GNY transition. This conclusion is one of our main results.

Motivated by the above results, we now extract the critical properties of the OSM confinement transition from the numerical data. The dimensionless susceptibility ratios are expected to follow a simple scaling form $\lambda_{\text{AFM/VBS}}(h, L) = \tilde{\lambda}_{\text{AFM/VBS}}(\delta h L^{1/\nu})$, where $\delta h = h - h_c$ defines the quantum detuning parameter from the critical coupling h_c , and ν is the correlation length exponent. In Figs. 4a and 4b we present the universal scaling functions $\tilde{\lambda}_{\text{AFM/VBS}}$ obtained from a curve collapse analysis using $h_c = 0.69(2)$ and $\nu = 0.58(1)$.

In the presence of $SO(5)$ symmetry, the AFM and VBS order parameters are expected to share the same anomalous exponent η . We assume the standard scaling form $\chi_{\text{VBS/AFM}} = L^{2-\eta} \tilde{\chi}_{\text{VBS/AFM}}(\delta h L^{1/\nu})$, where $\tilde{\chi}_{\text{VBS/AFM}}$ are the universal scaling functions of the VBS and AFM order parameters. In Figs. 4c and 4d we depict the universal scaling functions $\tilde{\chi}_{\text{VBS/AFM}}$ using our previous estimates for h_c and ν and the *same* anomalous exponent $\eta = 1.4(1)$. The increased system size and improved methodology used in this work allowed for a more reliable determination of critical exponents, compared to the ones appearing in Ref. [25].

In the above scaling analysis, we found that curves corresponding to the smallest system sizes deviate from the expected universal curve. These scaling violations are most likely attributed to non-universal corrections to scaling that may be sizable at small system sizes. Nevertheless, we note that the critical regime over which we obtain a nearly perfect curve collapse systematically increases with the systems size.

We note that although the AFM and VBS exponents co-incide, the scaling functions, $\tilde{\chi}_{\text{VBS/AFM}}$, in Figs. 4c and 4d do not appear to be the same. The theory to be presented in Section IV requires these functions to be the same at leading order, with differences only appearing upon considering corrections to scaling. This feature needs to be understood better in future work.

IV. CRITICAL THEORY OF THE CONFINEMENT TRANSITION

A. Previous work

It is useful to first recall other theories of confinement transitions out of a state with \mathbb{Z}_2 topological order [46]. The confinement transition of the even ILGT without dynamical matter was already described by Wegner [2], which he showed was in the (inverted) Ising universality class. The odd ILGT without dynamical matter has a confinement transition to a state with VBS order, and the square lattice critical point is described by a deconfined $U(1)$ gauge theory [5, 7, 47]. This can be understood by viewing the \mathbb{Z}_2 gauge theory of the topological state as a compact $U(1)$ gauge theory in which a charge 2 Higgs field has condensed [48]. Then the uncondensing of the Higgs field leads to a confining phase of the $U(1)$ gauge theory, across a critical point where the $U(1)$ gauge fields are deconfined: the background \mathbb{Z}_2 electric charges of the odd ILGT suppress the $U(1)$ monopoles at the critical point, leading to deconfinement. This furnishes an example of an enlarged gauge group appearing at the confinement-deconfinement critical point of a \mathbb{Z}_2 gauge theory. Analogously, we will see that for our problem of confinement of ILGT coupled to massless fermions, enlarging the gauge group can account for this transition as well. However, here we will need to introduce an $SU(2)$ gauge symmetry as described below.

B. Fractionalization and Higgs field: parton construction

The f fermions that appear in the Ising gauge theory can be constructed via the following ‘parton’ construction by fractionalizing the physical, gauge invariant degrees of freedom. Notice, the gauge invariant operators in that model are purely bosonic, and include the spin \mathbf{S} and psuedospin \mathbf{I} generators. The latter include the $U(1)$ charge operators I^z , and I^\pm that create/destroy charged bosons. These can be decomposed into partons as follows. First define:

$$X_r = \begin{pmatrix} f_{r\uparrow} & -f_{r\downarrow}^\dagger \\ f_{r\downarrow} & f_{r\uparrow}^\dagger \end{pmatrix} \quad (4.1)$$

The spin and psuedospin rotations act via multiplication of $SU(2)$ matrices to the right or left: $X \rightarrow U^s X [U^{ps}]^\dagger$. Then the physical operators are:

$$\mathbf{S}_r = \frac{1}{4} \text{Tr}\{X_r^\dagger \boldsymbol{\tau} X_r\}; \quad \mathbf{I}_r = \frac{1}{4} \text{Tr}\{X_r \boldsymbol{\mu} X_r^\dagger\} \quad (4.2)$$

Here we are using the convention for spin/pseudospin Pauli matrices $\boldsymbol{\tau}/\boldsymbol{\mu}$ from Eq. (3.1). Clearly there is a \mathbb{Z}_2 gauge redundancy in this definition corresponding to changing the sign of the fermion operators. Thus a minimal parton Hamiltonian will have hopping of f fermions mediated by an

Ising (\mathbb{Z}_2) gauge field, as in to our starting model. However, in order to accomplish the observed transition we will need a different set of variables. To this end, define a fermion matrix field Y_r which is superficially similar to the X_r above, however which only carries the spin quantum number. The psuedospin is assumed to be carried by a triad of bosonic matrix fields \hat{H}_a , $a = 1, 2, 3$ each of which is a 2×2 matrix. This can also be written as $\hat{H}_a = \sum_{b=1}^3 H_{ab} \mu^b = \vec{H}_a \cdot \vec{\mu}$. In terms of these fields we can decompose the physical operators as:

$$\mathbf{S}_r = \frac{1}{4} \text{Tr}\{Y_r^\dagger \boldsymbol{\tau} Y_r\}; \quad I_{ar} = \frac{1}{4} \text{Tr}\{Y_r \hat{H}_{ar} Y_r^\dagger\} \quad (4.3)$$

While spin rotations are implemented as before $Y \rightarrow U^s Y$, psuedospin rotations only act on \hat{H}^a which transforms as a vector. This decomposition though has additional gauge freedom, for instance we can simultaneously rotate:

$$Y_r \rightarrow Y_r [U_r^g]^\dagger; \quad \hat{H}_{ar} \rightarrow U_r^g \hat{H}_{ar} [U_r^g]^\dagger \quad (4.4)$$

which leaves the physical operators invariant. Therefore this decomposition has an $SU(2)$ gauge redundancy. Therefore the effective theory will now involve Y fermions coupled to an $SU(2)$ gauge field. We can readily recover the \mathbb{Z}_2 Dirac phase as follows. Consider a Higgs transition in which the fields H_{ab} acquire an expectation value:

$$\langle H_{ab} \rangle = H_0 \delta_{ab}. \quad (4.5)$$

Then, $\hat{H}_a = H_0 \mu^a$ and Eq. (4.3) reduces to Eq. (4.2). We will later see that the dynamics at the transition will naturally favor such a Higgs condensate.

C. Fractionalization and Higgs field: Rotating reference frame construction

An alternate derivation of the fractionalized degrees of freedom can be obtained by first expanding the Hilbert space of the model to include electron excitations c_α . We can then show that the AFM and VBS order parameters of the possible confining phases, and the orthogonal fermions f_α of the \mathbb{Z}_2 deconfined phase, all emerge by transforming the underlying gauge-invariant electrons, c_α , to a rotating reference frame under $SU_c(2)$.

A similar approach was adopted in Refs.[49, 50] which considered phases with \mathbb{Z}_2 topological order in which there are dynamical fermions carrying \mathbb{Z}_2 gauge charges and the global $U_c(1)$ charge ($U_c(1)$ is a subgroup of $SU_c(2)$), but these fermions are spinless under $SU_s(2)$. The transition of these phases to confining Fermi liquids (which can be unstable to superconductivity) was described by embedding the \mathbb{Z}_2 gauge theory in a $SU(2)$ gauge group. This larger gauge group was needed for a proper description of the confining phase in terms of composites of the fractionalized degrees of freedom [51]. It was introduced by transforming to a ‘rotating reference frame’ under $SU_s(2)$. In

the topological phase, the $SU(2)$ gauge invariance was broken down to \mathbb{Z}_2 by condensing a $SO(3)$ Higgs field which was neutral under $U_c(1)$ and $SU_s(2)$.

In our case, we transform to a rotating reference frame under $SU_c(2)$ by writing [52, 53]

$$\begin{pmatrix} c_{r,\uparrow} \\ c_{r,\downarrow}^\dagger \end{pmatrix} = R_r \begin{pmatrix} f_{r,\uparrow} \\ f_{r,\downarrow}^\dagger \end{pmatrix} \quad (4.6)$$

where R_r is a position and time dependent $SU(2)$ matrix which performs the transformation to a $SU_c(2)$ rotating reference frame. This definition immediately introduces a $SU_g(2)$ gauge invariance because the r.h.s. is invariant under

$$R_r \rightarrow R_r U_r^g \quad , \quad \begin{pmatrix} f_{r,\uparrow} \\ f_{r,\downarrow}^\dagger \end{pmatrix} \rightarrow [U_r^g]^\dagger \begin{pmatrix} f_{r,\uparrow} \\ f_{r,\downarrow}^\dagger \end{pmatrix} \quad , \quad (4.7)$$

where U_r^g is an arbitrary spacetime-dependent $SU_g(2)$ matrix, as in Eq. (4.3). The definition in Eq. (4.6) shows that R_r transforms as a $SU_c(2)$ fundamental under left multiplication, and a $SU_g(2)$ fundamental under right multiplication. Note that in this $SU_g(2)$ gauge theory formulation, and unlike the \mathbb{Z}_2 gauge theory in Eq. (2.2), at this point the f fermions do not carry a $SU_c(2)$ charge; they only carry a $SU_g(2)$ charge, and the $SU_c(2)$ charge has been transferred from the f to the R .

We now want to obtain an OSM state, proximate to confining AFM/VBS states, from the $SU_g(2)$ gauge theory defined by Eq. (4.6). Condensing the R boson would completely Higgs $SU_g(2)$, and so we assume that R remains gapped across the transition. But we can break $SU(2)$ down to \mathbb{Z}_2 by condensing a matrix Higgs field, H_{ab} , which is composed of a pair of R bosons:

$$H_{ab} \sim \text{Tr} (\mu^a R \mu^b R^\dagger) \quad , \quad (4.8)$$

where $a, b = 1, 2, 3$. This is an alternative interpretation of the Higgs field H_{ab} introduced in the Section IV B. Eq. (4.8) is the analog of the paired condensate of ‘slave’ bosons carrying $U(1)$ gauge charges in the OM construction of Ref. [26]. H_{ab} transforms as spin-one under the $SU_g(2)$ gauge and $SU_c(2)$ pseudo-spin symmetries via a left and right multiplications, respectively.

Now introducing a Higgs condensate as in Eq. (4.5) breaks the gauge $SU_g(2)$ down to \mathbb{Z}_2 . It also ties together the global $SU_g(2) \times SU_c(2)$ transformations to a diagonal subgroup, so that the f fermions effectively acquire a $SU_c(2)$ index. These are precisely the characteristics of the observed OSM phase.

We note that the Higgs field in Eq. (4.8) is the only possible R pair without spatial gradients. Other possibilities for R pair Higgs fields are either trivial ($\text{Tr} (RR^\dagger) = 2$) or vanish identically ($\text{Tr} (\mu^a RR^\dagger) = \text{Tr} (R \mu^b R^\dagger) = 0$). We can also make Higgs fields from pairs of the f fermions, as was done recently in Ref. [54]. Such Higgs fields carry only $SU_g(2)$ charges, and their condensation leads to topologically ordered phases with fermionic excitations with global $SU_s(2)$ charges only: these are not orthogonal fermions, and so condensation of the f pair Higgs field does not lead to an OSM.

D. Critical theory

We can now write down a continuum theory for a phase transition out of the OSM phase by assembling the degrees of freedom described above in a $SU_g(2)$ gauge theory. First we take the continuum limit of the $(f_\uparrow, f_\downarrow)$ fermions moving in a π flux background to obtain two-components Dirac spinors, ψ_v , which carry a valley index $v = 1, 2$ and a fundamental $SU_g(2)$ gauge charge (index not explicitly displayed). The fermions also carry a $SU_s(2)$ charge, but its action is clearer in a Majorana fermion representation [18, 54]. Minimally coupling these fermions to a $SU_g(2)$ gauge field, we obtain two-color QCD coupled to $N_f = 2$ flavors of Dirac fermions in three space-time dimensions. This theory was examined recently by Wang *et al.* [18], and following them we dub it $\text{QCD}_3(N_f = 2)$.

Wang *et al.* noted that $\text{QCD}_3(N_f = 2)$ has a global $SO(5)$ symmetry, and that a gauge-invariant fermion bilinear transforms as an $SO(5)$ vector. Tracing this fermion bilinear back to the lattice fermions, f_α , they noted that this $SO(5)$ order parameter is precisely the composite of the 3-component AFM order parameter and the 2-component VBS order parameter. A confining phase of QCD_3 is expected to break the $SO(5)$ symmetry, and so we have achieved our aim of writing down a theory which is proximate to confining phases with AFM or VBS order. We have also obtained an understanding of the evidence for $SO(5)$ symmetry in our numerics.

Finally, we combine $\text{QCD}_3(N_f = 2)$ with a phenomenological action for H to obtain our theory for the transition between the OSM and AFM phases.

$$\begin{aligned} \mathcal{S} = & \int d^3x \sum_{v=1}^{N_f} \bar{\psi}_v \not{D}_a \psi_v - \frac{1}{2} \text{Tr} \left[(D_a^H H)^T (D_a^H H) \right] \\ & + \frac{1}{2} m^2 \text{Tr}[H^T H] + \kappa \det H + \frac{1}{4} \lambda \text{Tr}[H^T H]^2 \\ & + \frac{1}{4} \lambda' \text{Tr}[(H^T H)^2] + \frac{1}{4} f_{\mu\nu}^2. \end{aligned} \quad (4.9)$$

Here a_μ^c represents the $SU(2)$ gauge field, and the covariant derivative of the Dirac fermions is defined as $\not{D}_a = \gamma_\mu (i\partial_\mu + a_\mu^c \tau^c)$, where τ^c are the Pauli matrices. Similarly, the covariant derivative of the Higgs field reads, $D_a^H = (\partial_\mu + a_\mu^c O^c)$, where O^c are the generators of $SO(3)$ rotations. Finally, the last term is the standard Maxwell term, with $f_{\mu\nu}^c$ being the non-abelian field strength. Note that all terms in Eq. (4.9) respect the global $SO(5)$ symmetry.

The transition between OSM and AFM phases is described by tuning the Higgs mass, m^2 , as shown in Fig. 5. For negative m^2 , the Higgs field is condensed as in Eq. (4.5), and we obtain an OSM phase as described above. Note that the ψ_v fermions remain massless even when the Higgs field is condensed. This is because there is no allowed tri-linear Yukawa term between the Higgs boson and the fermions; such a Yukawa term is forbidden by $SU_c(2)$ symmetry, as the matrix Higgs

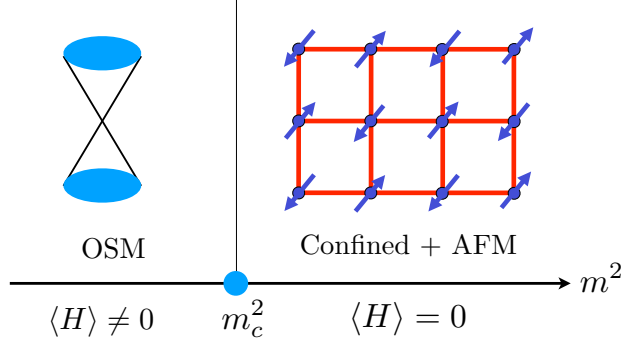


FIG. 5: Higgs mediated confinement transition. For positive Higgs mass, $m^2 > 0$, the Higgs field is gapped. The effective field theory is then $\text{QCD}_3(N_f = 2)$, which confines and spontaneously breaks chiral symmetry, leading to an insulator with AFM order. Conversely, for $m^2 < 0$, the Higgs field condenses and reduces the $SU_g(2)$ gauge symmetry down to \mathbb{Z}_2 giving rise to the OSM.

field H carries a $SU_c(2)$ charge, while the fermions ψ do not. This feature is in contrast to earlier theories of phases with \mathbb{Z}_2 topological order [49, 50, 54], where the Yukawa term was symmetry allowed, and led to a gap in the fermion spectrum when the Higgs field was condensed.

For positive m^2 , we can neglect the massive Higgs field, and then Eq. (4.9) reduces to $\text{QCD}_3(N_f = 2)$. For sufficiently large N_f , $\text{QCD}_3(N_f)$ defines a deconfined conformal field theory, with non-trivial scaling dimensions that can be computed in a $1/N_f$ expansion. However, it is expected that there is a critical N_f^c such that for $N_f < N_c$ the theory is confining. The most recent lattice QMC calculation [55] estimates $N_f^c = 4 - 6$. For $N_f = 2$, which is relevant to our case, a clear ‘chiral’ symmetry breaking was observed, corresponding to a breaking of $SO(5)$ symmetry in our language. [56] Therefore, in Eq. (4.9), the Higgs transition provides a means to simultaneously drive confinement and symmetry breaking using a *single* tuning parameter corresponding to the mass-squared of the Higgs field. Once we are in the $SO(5)$ -broken regime, other irrelevant operators (not shown in Eq. (4.9)) will become important, and we assume these select the AFM order observed, rather than the VBS order.

Finally we turn to the critical point between the OSM and AFM phases. We assume that this is described by the $SO(5)$ -symmetric deconfined critical theory in Eq. (4.9) after the Higgs mass m^2 has been tuned to its critical value. The idea is that the additional contributions of the critical Higgs modes, when combined with the gapless fermions, are sufficient to suppress the confining effects of the $SU_g(2)$ gauge field. The continuous transition observed in our numerics, along with the evidence for global $SO(5)$ symmetry is evidence in support of our proposal.

We note also the cubic term, proportional to κ in Eq. (4.9). In purely scalar field theories, this would be sufficient to imply a first-order phase transition. However, when combined with strong gauge fluctuations and massless fermions, it is not clear whether estimates which expand about the

upper-critical dimension can be reliable. In the large- N_f expansion of such a Higgs critical theory, the κ determinant term involves of order N_f powers of the Higgs field, and is clearly irrelevant at the critical point. Our evidence for a continuous transition is evidence that this is also likely the case at $N_f = 2$.

Even if irrelevant at criticality, on moving into the Higgs phase, the κ determinant term will dictate the nature of the Higgs condensate. Note, that since multiple Higgs fields are present due to the global symmetry, different patterns of Higgs condensates are possible depending on how many \hat{H}_a we condense. These are all degenerate to quadratic order, but are differentiated by the determinant term that selects a simultaneous condensate as in Eq. (4.5) independent of the sign of κ . This form of the Higgs condensate is crucial to obtaining the OSM phase.

V. DISCUSSION AND SUMMARY

We have carried out a detailed numerical analysis of the confinement transition of the orthogonal semi-metal (OSM) in a model with a repulsive on-site Hubbard interaction. This serves as a model of a confinement transition in a \mathbb{Z}_2 gauge theory coupled to gapless Dirac fermions that carry gauge charge, which is also free of the fermion sign problem. Our key numerical finding is an emergent $SO(5)$ symmetry at criticality that enlarges the microscopic $SO(3) \times C_4$ symmetry associated with spin rotations and the discrete square lattice point group symmetry. Crucially, we demonstrate that this result is a qualitatively unique feature of the OSM confinement transition that fundamentally distinguishes it from the more conventional Gross-Neveu-Yukawa (GNY) and Ising criticality. In addition, our refined numerical calculations allowed us to improve previous estimates of critical data, and further support the scenario of deconfined criticality (DC) with a second order phase transition.

We note that, even more than a decade after the initial theoretical proposal, the ultimate thermodynamic fate of DC for insulating square lattice antiferromagnets remains in debate. Numerical studies of lattice models show conflicting results, where estimates of certain universal quantities exhibit a significant drift with system size, and in certain models even an indication for a first order transition. On the other hand, several numerical studies indicate an enlarged $SO(5)$ symmetry that is hard to reconcile with a first order transition (see Ref.[18] for a recent discussion).

As our model involves fermionic degrees of freedom, its computational cost using standard QMC methodology does not scale favorably with systems size, compared to models of non-LGW transitions consisting of bosonic degrees of freedom. It is therefore more challenging to assert a strong statement on the thermodynamic limit of our model. Nevertheless, up to the largest length scale studied, we did not observe any sign of deviation from critical scaling and critical properties seem to remain robust for a wide range of microscopic parameters without any degree of fine

tuning. Most relevant for this work, it is difficult to imagine a scenario, in which an enlarged symmetry could generically arise at a first order phase transition.

We used the numerical results as a guide for constructing a field theory description of the OSM confinement transition, which is linked to recent studies of descended phase of $\text{QCD}_3(N_f = 2)$ [12, 13, 18, 54]. We introduced a *matrix* Higgs mechanism, which is distinct from the vector Higgs approach presented in Ref. [54]. In the latter case, the Higgs fields were bilinears of the fermions f_α , in contrast to the boson bilinears we employed in Eq. (4.8), and their condensation led to spin liquids with fermionic spinons which do not carry the electromagnetic charge. In contrast, condensation of our matrix Higgs field led to an orthogonal metal, in which the fermions carry both spin and electromagnetic charge. At the same time the fermions carry \mathbb{Z}_2 gauge charge, unlike in the symmetric mass generation scenario of Refs. [12, 13], where a Higgs field in the fundamental representation condenses giving rise to gapless fermions, without gauge charge.

Looking to the future, it would be interesting to explore some extension of our Higgs mechanism. Our QCD_3 mechanism has a natural prediction when time-reversal symmetry is explicitly broken, in which case the Dirac fermions obtain a mass term with total Chern number $C = 2$. Deep in the deconfined phase this leads to a Semion \times Semion topological order ($\nu = 4$ in Kitaev's 16-fold classification [15]). However, near the critical point (when the Chern mass scale is greater than the Higgs mass scale), we obtain an $SU(2)_1$ Chern-Simons theory which is simply the Semion chiral spin liquid. The two topological orders can in principle be distinguished by their ground state degeneracy on a torus or infinite cylinder, perhaps through DMRG calculation. This Semion topological order, if observed, would be a strong signature of the enhanced gauge symmetry near the critical point.

Another extension, which may be implemented in quantum Monte Carlo, is to consider similar transitions described by QED_3 , namely a $U(1)$ (instead of $SU(2)$) gauge theory coupled to $N_f = 4$ Dirac fermions. There are two scenarios in which this would be natural. First, one could consider explicitly breaking the pseudo-spin $SU_c(2)$ symmetry down to $U(1)$, say by breaking the particle-hole symmetry. Alternatively, one can study a similar system but with \mathbb{Z}_4 gauge field on the lattice – in fact in this scenario we can have more controlled arguments about the ultimate IR fate of the phases and phase transition, as we briefly outline in Appendix D. In both cases the gauge symmetry can be naturally enlarged to $U(1)$ but not $SU(2)$. At the critical point of such QED_3 -Higgs transition we expect an enlarged $SO(2) \times (SO(6) \times U(1))/\mathbb{Z}_2$ symmetry, instead of $SO(3) \times SO(5)$ in the QCD_3 -Higgs transition (the Neel-VBS $SO(5)$ observed in this work is a subgroup of both symmetries).

On the numerical front, we see several exciting future directions. First, identifying observables that can probe the emergent $SU(2)$ gauge fields and matrix Higgs field, H , would allow for direct confirmation of the critical theory in the numerical simulations. Second, the emergence of an $SO(5)$

symmetry at criticality can be further tested by studying certain high order correlation functions that are required to vanish by symmetry [19]. Finally, eliminating the observed non-universal corrections to scaling requires simulations on larger lattices, beyond standard methodologies. In that regard, one promising approach is the Hamiltonian variant of the fermion bag algorithm [57, 58].

Lastly, we note that since the theory we simulated, \mathcal{H} , does not contain any gauge neutral fermion it can be thought of arising from an underlying bosonic theory. It is tempting to conjecture that the associated bosonic description will also be free of the numerical sign problem. Identifying such bosonic lattice models would allow access to significantly larger system sizes and an accurate study of critical properties.

Acknowledgements

We thank Shubhayu Chatterjee, Tarun Grover and Mathias Scheurer for valuable discussions: SC and MS pointed out that the $\det H$ term in Eq. (4.9) was allowed. SG and AV thank Mohit Randeria for an earlier collaboration on a related topic. The authors gratefully acknowledge the Gauss Centre for Supercomputing e.V. (www.gauss-centre.eu) for funding this project by providing computing time on the GCS Supercomputer SuperMUC at Leibniz Supercomputing Centre (www.lrz.de). FFA thanks the DFG through SFB 1170 ToCoTronics for financial support. This research was supported by the National Science Foundation under Grant No. DMR-1360789 (SS). Research at Perimeter Institute is supported by the Government of Canada through Industry Canada and by the Province of Ontario through the Ministry of Research and Innovation. SS also acknowledges support from Cenovus Energy at Perimeter Institute. SG was supported by the ARO (W911NF-17-1-0606) and the ERC Synergy grant UQUAM. This work was partially performed at the Aspen Center for Physics (NSF grant PHY-1607611) and the Kavli Institute for Theoretical Physics (NSF grant PHY-1125915). AV was supported by a Simons Investigator Grant, and AV and SG were supported by NSF DMR- 1411343. CW was supported by the Harvard Society of Fellows. This research used the Lawrence computational cluster resource provided by the IT Division at the Lawrence Berkeley National Laboratory (Supported by the Director, Office of Science, Office of Basic Energy Sciences, of the U.S. Department of Energy under Contract No. DE-AC02-05CH11231)

Appendix A: Circumventing the zero mode problem at finite Hubbard interactions

To enforce Gauss's law in the numerical simulation [25], we introduce a set of discrete Lagrange multipliers, λ_r , at each lattice site, r , which are identified with the temporal component of the

Ising gauge field. Explicitly, for an even LGT $G_r = 1$, we project to the physical Hilbert space using the projector $\hat{P} = \prod_r \hat{P}_r$, where,

$$\begin{aligned}\hat{P}_r &= \frac{1}{2} \left(1 + \prod_{b \in +_r} \sigma_{r,b}^x (-1)^{n_r^f} \right) \\ &= \sum_{\lambda_r = \pm 1} e^{i\pi \left(\frac{1-\lambda_r}{2} \right) \left(\sum_{b \in +_r} \left(\frac{1-\sigma_{r,b}^x}{2} \right) + n_r^f \right)}.\end{aligned}\tag{A1}$$

Substituting the above expression in the path integral representation yields the following fermionic weight (see [25] for a complete derivation),

$$W_f(\lambda, \sigma^z) = \text{Tr} \left[e^{i\pi \sum_r \left(\frac{1-\lambda_r}{2} \right) n_r^f} \prod_{\tau} e^{f^\dagger K(\sigma^z(\tau)) f} \right].\tag{A2}$$

In the above, $K(\sigma^z(\tau))$ is the infinitesimal $\sigma^z(\tau)$ -dependent hopping kernel. Remarkably, the constraint does not introduce a sign problem for an arbitrary fermion density. However, at half-filling, configurations satisfying $\prod_r \lambda_r = -1$ sustain an exact zero mode, as can be verified by applying a partial PH symmetry to Eq. (A2). Such configurations have a vanishing Boltzmann weight and are not sampled in the Monte Carlo simulation.

This introduces a systematic bias in expectation values of observables that are not symmetric under partial PH transformation. In Ref. [25], a method that compensates on the missing weight was presented.

In the present work, we consider a simpler solution, explained below. The Hubbard term is decoupled using an auxiliary-field s_r . For attractive interactions the density channel decoupling is given by,

$$e^{\epsilon U (n_r^\uparrow - \frac{1}{2})(n_r^\downarrow - \frac{1}{2})} = \frac{1}{2} \sum_{s=\pm 1} e^{\gamma s_r (n_r^\downarrow + n_r^\uparrow - 1)}\tag{A3}$$

where $\gamma = \cosh^{-1}(\exp(\epsilon U/2))$. It is clear from the above equation that the associated weight is not symmetric under partial PH transformation for a *generic* auxiliary-field configuration. Therefore for finite Hubbard interactions, the zero mode is lifted allowing for an accurate sampling. We have verified this fact explicitly by benchmarking the QMC data with exact diagonalization on small system sizes.

Appendix B: Additional QMC data

In this section, we present additional QMC data supporting our finding in the main text. In Fig. 6, we consider two parameter cuts corresponding to the AFM ordering transition between the OSM and AFM* phases and the Ising confinement transition between the AFM* and AFM

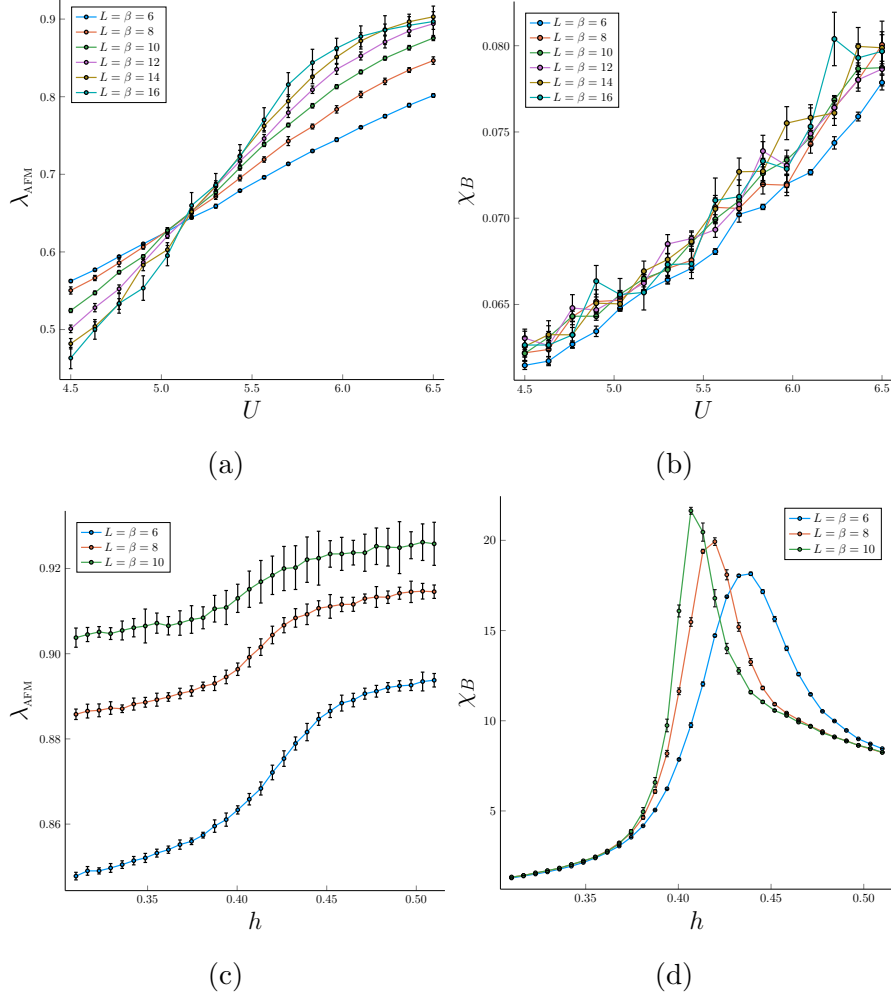


FIG. 6: (a-b) AFM ordering transition separating the AFM* and OFM phases. QMC data is calculated at $h = 0.1$ and as a function of U . (a) λ_{AFM} exhibits a clear curve crossing (b) χ_B crosses the transition smoothly. (c-d) Ising confinement transition separating the AFM* and AFM phases. QMC data is calculated at $U = 7$ and as a function of h . (c) λ_{AFM} , indicates that the AFM order remains finite across the transition. (d) The Ising flux susceptibility, χ_B , diverges at the confinement transition with increase in the system size.

phases. As expected, we find that the former involves only AFM ordering as seen in a curve crossing analysis of λ_{AFM} , while the latter is marked solely by a singularity in flux susceptibility, χ_B , indicating confinement.

Finally, in Fig. 7, we depict the joint probability distribution, $\mathbf{P}(\mathbf{B}^x, \mathbf{B}^y)$, of the VBS order parameter along the x and y directions, evaluated at the OSM confinement transition. The visible circular symmetry supports the emergence of rotational $SO(2)$ symmetry at the OSM confinement transition.

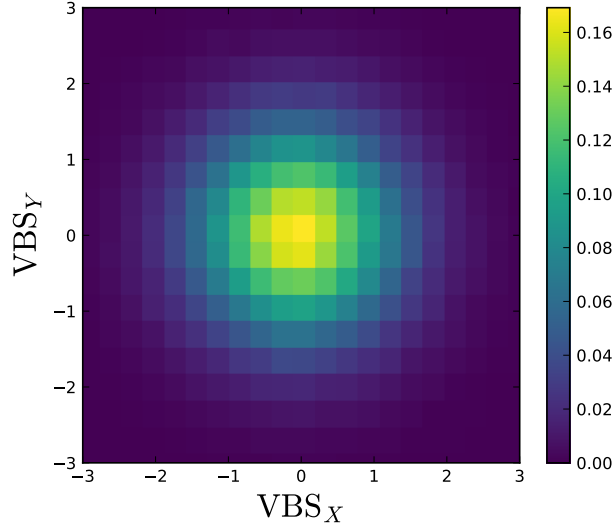


FIG. 7: Joint probability distribution $\mathbf{P}(\mathbf{B}^x, \mathbf{B}^y)$ at the OSM confinement transition. The apparent circular symmetry indicates that the C_4 square lattice symmetry is enlarged to an $SO(2)$ rotational symmetry.

Appendix C: Dynamically imposed constraint

Imposing the constraint $Q_r = \pm 1$ is necessary to satisfy local \mathbb{Z}_2 gauge symmetry. In fact, without a constraint the model is very asymmetric in space and time: $\langle f_{r,\alpha}^\dagger(\tau) f_{r',\alpha'}(\tau = 0) \rangle = \delta_{r,r'} \delta_{\alpha,\alpha'}$. Since G_r commutes with the Hamiltonian, the constraint will be dynamically imposed in the low temperature limit and for observables satisfying $[O, G_r] = 0$, we expect:

$$\lim_{L \rightarrow \infty} \lim_{T \rightarrow 0} \langle O(\tau) O \rangle_{NC} = \lim_{L \rightarrow \infty} \lim_{T \rightarrow 0} \langle O(\tau) O \rangle_C. \quad (\text{C1})$$

Thus, provided that we first take the zero temperature limit on a finite sized lattice, simulations with, $\langle \bullet \rangle_C$, or without, $\langle \bullet \rangle_{NC}$, constraint should converge to the same result. It is very hard to realize this ordering of limits numerically: as $h \rightarrow 0$ the relevant energy scale below which the constraint is dynamically imposed vanishes. Above this energy scale, the Ising fields freeze. The model without constraint is amenable to sign free QMC simulations at odd flavors and may be easier to simulate with alternative methods such as the fermion bag approach [58]. It is hence certainly worth while comparing results with and without constraint. In this appendix, we briefly present QMC data where the constraint is not explicitly taken into account, and show that consistent results are obtained. We have used the ALF implementation of the auxiliary field QMC algorithm [39]. In contrast to data presented in Ref. [24], we have used parallel tempering schemes as well as global updates to flip blocks of spins along the imaginary time. These approaches aim at reducing

the long autocorrelation times we encounter in the vicinity of the OSM to AFM transtion. Fig. 8 shows the phase diagram at $J/t = -1$ in the U - h plane. We fix the temperature to $\beta t = 80$ such that, as mentioned above, and in the low- h limit the Ising fields freeze and we recover results of the π -flux Hubbard model [35].

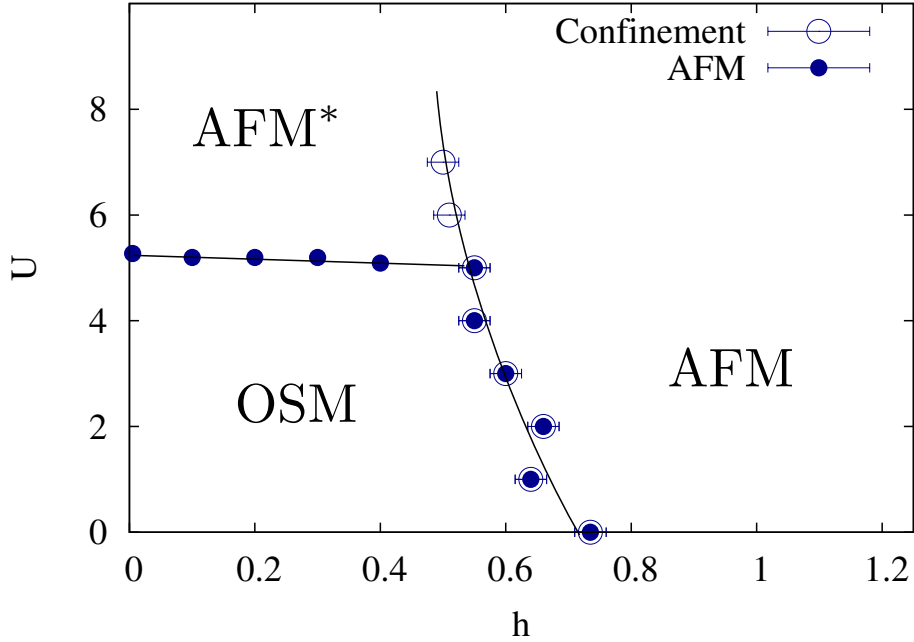


FIG. 8: Phase diagram at $J/t = -1$. Data stems from simulations at $L = 10$ and $L = 14$. The AFM transition is obtained by analyzing the renormalization group invariant quantity λ_{AFM} . The confinement transition is obtained by monitoring $\chi_B = \partial\langle\Phi\rangle/\partial h$. We have equally checked that at the confinement transition, visons proliferate. We have used values of $\Delta\tau = 0.4, 0.2, 0.1$ for growing values of U/t .

Figs. 9 and 10 plot the VBS and AFM correlation ratios, λ_{AFM} and λ_{VBS} as obtained from the susceptibilities. Both λ_{AFM} and λ_{VBS} are renormalization group invariant quantities and are expected to cross at the critical point. This relies on the assumption that the susceptibility is dominated by the singular part of the free energy and thereby requires $\eta < 2$. Note that the finite size scaling form for susceptibilities reads $\chi \simeq L^{2-\eta} G(L^z/\beta, L^{1/\nu}(g - g_c))$. Fig. 9(a) shows λ_{AFM} for the O(3)-Gross-Neveu-Yukawa transition [34–36] and clearly pins down the critical value of U/t . The data of Fig. 9(b) is consistent with a constant value of λ_{VBS} at the transition and in the thermodynamic limit thereby confirming critical VBS fluctuations at the transition. However, the quotient χ_{VBS}/χ_{AFM} clearly shows that at the O(3)-Gross-Neveu-Yukawa transition $\eta_{VBS} > \eta_{AFM}$

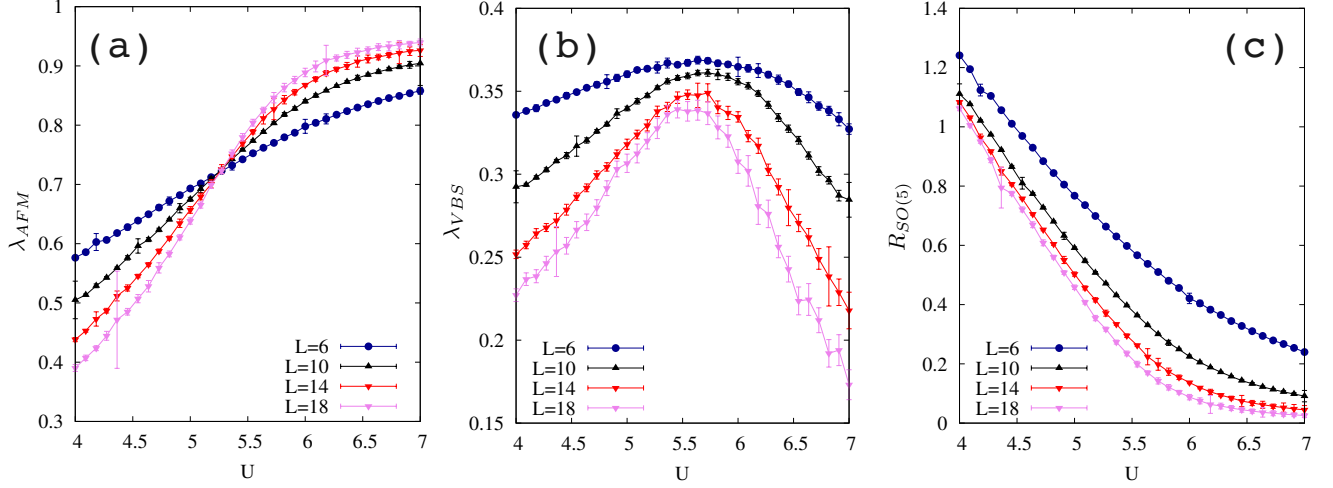


FIG. 9: Simulations were carried out at $L = \beta$, $h/t = 0.05$, and $\Delta\tau t = 0.1$. For this choice of h and βt the Ising field are essentially frozen and the flux per plaquette is very close to -1. (a) λ_{AFM} as obtained from the susceptibilities. (b) λ_{VBS} as obtained from the susceptibilities. (c) Ratio $R_{\text{SO}(5)} = \chi_{\text{VBS}}/\chi_{\text{AFM}}$.

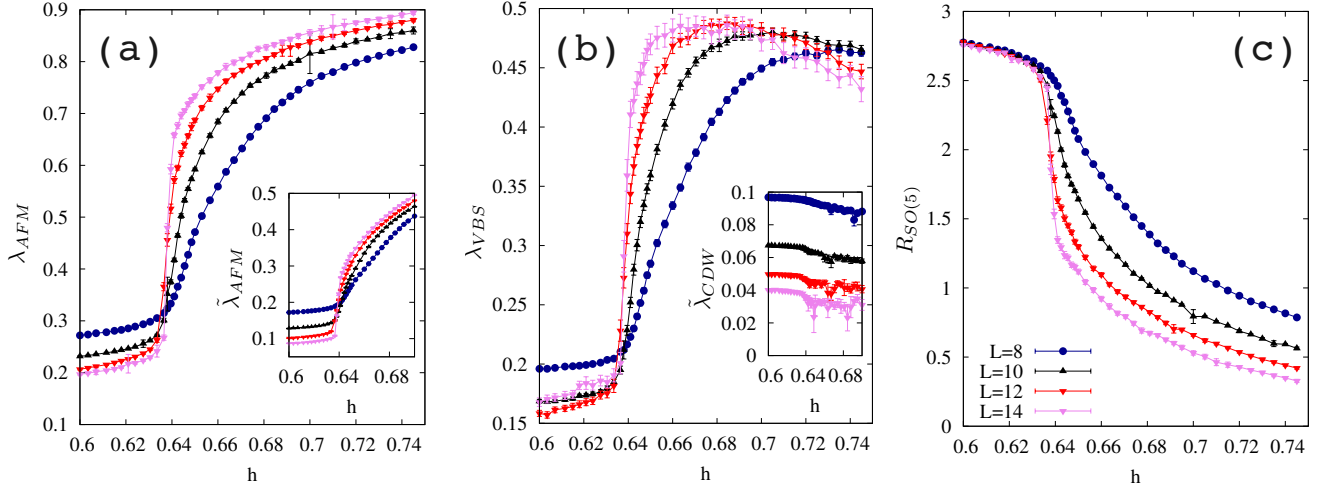


FIG. 10: Simulations are carried out at $\beta t = 80$, $U/t = 1$, $\Delta\tau = 0.4$. The temperature was chosen as low as possible so as to attempt to satisfy the constraint. (a) λ_{AFM} as obtained from the susceptibilities. Inset: $\tilde{\lambda}_{\text{AFM}}$ as obtained from equal time correlation functions. (b) λ_{VBS} as obtained from the susceptibilities. Inset: Charge density wave (CDW) correlation ratio at the antiferromagnetic wave vector, $\tilde{\lambda}_{\text{CDW}}$, as obtained from equal time correlation functions. (c) Ratio $R_{\text{SO}(5)} = \chi_{\text{VBS}}/\chi_{\text{AFM}}$.

since at U_c , the curves fail to cross. Such a statement does not hold for the OSM to AFM transition (see Fig. 10). Here, the data is consistent with $\eta_{\text{VBS}} = \eta_{\text{AFM}}$ thereby supporting an emergent $\text{SO}(5)$ symmetry. The inset of Fig. 10(a) shows the AFM correlation ratio – as obtained from equal time correlation functions. Comparison with the equivalent data for the charge density wave (CDW), inset of Fig. 10(b), shows that the $\text{SO}(8)$ symmetry of Dirac fermions is violated at the OSM to AFM transition.

Appendix D: QED₃ and confinement transition of \mathbb{Z}_4 gauge theory

We consider the following continuum theory

$$\mathcal{L} = \sum_{i=1}^4 \bar{\psi}_i \not{D}_a \psi_i + \frac{1}{2} |D_{4a} \phi|^2 + r |\phi|^2 + \lambda |\phi|^4 + \frac{1}{4e^2} f_{\mu\nu}^2 + \kappa V + \kappa^* V^*, \quad (\text{D1})$$

where a_μ is a $U(1)$ gauge field, ψ_i is a two-component Dirac fermion with gauge charge $q_g = 1$, ϕ is a complex boson with gauge charge $q_g = 4$, and V schematically represents the monopole (instanton) operator of the $U(1)$ gauge field.

Let us first ignore the monopole term. When $r < r_c$ the Higgs condensate $\langle \phi \rangle \neq 0$ will produce a \mathbb{Z}_4 gauge theory with $N_f = 4$ gapless Dirac fermions. When $r > r_c$ the Higgs field can be ignored at low energy, and we get a pure QED₃ with $N_f = 4$, which appears to be a stable conformal field theory from numerical studies [59]. The critical point is expected to be also stable since the extra critical Higgs field ϕ should further control the gauge field fluctuation. Therefore in the absence of monopole the above theory describes a continuous transition from $N_f = 4$ \mathbb{Z}_4 gauge theory to $N_f = 4$ QED₃.

Now put the monopole terms back (assuming such a term is compatible with all global symmetries, as supported by previous study [60]). For the Higgs phase this has no effect. For the QED₃ phase, the monopole term is likely relevant [61, 62] ($\Delta_V = 0.265N_f - 0.038 + O(1/N_f) = 1.022 + O(1/N_f) < 3$), and physically we expect confinement and spontaneous chiral symmetry breaking at low energy, producing a Neel-like state. At the critical point we expect the critical Higgs field to render the monopole irrelevant. This is because even without the gapless Dirac fermions, the monopole is known to be irrelevant because of the critical charge-4 Higgs field [63], and physically we expect the gapless Dirac fermions to make the monopole even more irrelevant. Therefore at the critical point the $U(1)$ gauge theory is effectively non-compact. Also notice that unlike the QCD₃ scenario for the transition studied in the main text, there is no cubic-like term for the Higgs field. For these reasons we expect the QED₃-Higgs theory to describe a continuous

transition is between a \mathbb{Z}_4 gauge theory with $N_f = 4$ Dirac fermions and a Neel state.

- [1] T. Senthil, A. Vishwanath, L. Balents, S. Sachdev, and M. P. A. Fisher, “Deconfined Quantum Critical Points,” *Science* **303**, 1490 (2004), [arXiv:cond-mat/0311326 \[cond-mat.str-el\]](#).
- [2] F. J. Wegner, “Duality in Generalized Ising Models and Phase Transitions without Local Order Parameters,” *Journal of Mathematical Physics* **12**, 2259 (1971).
- [3] X.-G. Wen and Y.-S. Wu, “Transitions between the quantum Hall states and insulators induced by periodic potentials,” *Phys. Rev. Lett.* **70**, 1501 (1993).
- [4] W. Chen, M. P. A. Fisher, and Y.-S. Wu, “Mott transition in an anyon gas,” *Phys. Rev. B* **48**, 13749 (1993), [cond-mat/9301037](#).
- [5] R. A. Jalabert and S. Sachdev, “Spontaneous alignment of frustrated bonds in an anisotropic, three-dimensional Ising model,” *Phys. Rev. B* **44**, 686 (1991).
- [6] A. V. Chubukov, T. Senthil, and S. Sachdev, “Universal magnetic properties of frustrated quantum antiferromagnets in two dimensions,” *Phys. Rev. Lett.* **72**, 2089 (1994), [cond-mat/9311045](#).
- [7] S. Sachdev and M. Vojta, “Translational symmetry breaking in two-dimensional antiferromagnets and superconductors,” *J. Phys. Soc. Jpn* **69**, Supp. B, 1 (1999), [cond-mat/9910231](#).
- [8] Y. BenTov, “Fermion masses without symmetry breaking in two spacetime dimensions,” *Journal of High Energy Physics* **2015**, 34 (2015).
- [9] V. Ayyar and S. Chandrasekharan, “Origin of fermion masses without spontaneous symmetry breaking,” *Phys. Rev. D* **93**, 081701 (2016).
- [10] S. Catterall, “Fermion mass without symmetry breaking,” *Journal of High Energy Physics* **2016**, 121 (2016).
- [11] Y.-Y. He, H.-Q. Wu, Y.-Z. You, C. Xu, Z. Y. Meng, and Z.-Y. Lu, “Quantum critical point of dirac fermion mass generation without spontaneous symmetry breaking,” *Phys. Rev. B* **94**, 241111 (2016).
- [12] Y.-Z. You, Y.-C. He, C. Xu, and A. Vishwanath, “Symmetric Fermion Mass Generation as Deconfined Quantum Criticality,” *Phys. Rev. X* **8**, 011026 (2018).
- [13] Y.-Z. You, Y.-C. He, A. Vishwanath, and C. Xu, “From bosonic topological transition to symmetric fermion mass generation,” *Phys. Rev. B* **97**, 125112 (2018).
- [14] T. Senthil and M. P. A. Fisher, “ \mathbb{Z}_2 gauge theory of electron fractionalization in strongly correlated systems,” *Phys. Rev. B* **62**, 7850 (2000), [cond-mat/9910224](#).
- [15] A. Kitaev, “Anyons in an exactly solved model and beyond,” *Annals of Physics* **321**, 2 (2006), [cond-mat/0506438](#).
- [16] A. Tanaka and X. Hu, “Many-Body Spin Berry Phases Emerging from the π -Flux State: Competition

- between Antiferromagnetism and the Valence-Bond-Solid State,” [Phys. Rev. Lett. **95**, 036402 \(2005\)](#), [cond-mat/0501365](#).
- [17] T. Senthil and M. P. A. Fisher, “Competing orders, nonlinear sigma models, and topological terms in quantum magnets,” [Phys. Rev. B **74**, 064405 \(2006\)](#), [cond-mat/0510459](#).
 - [18] C. Wang, A. Nahum, M. A. Metlitski, C. Xu, and T. Senthil, “Deconfined Quantum Critical Points: Symmetries and Dualities,” [Phys. Rev. X **7**, 031051 \(2017\)](#).
 - [19] A. Nahum, P. Serna, J. T. Chalker, M. Ortuño, and A. M. Somoza, “Emergent $SO(5)$ Symmetry at the Néel to Valence-Bond-Solid Transition,” [Phys. Rev. Lett. **115**, 267203 \(2015\)](#).
 - [20] H. Suwa, A. Sen, and A. W. Sandvik, “Level spectroscopy in a two-dimensional quantum magnet: Linearly dispersing spinons at the deconfined quantum critical point,” [Phys. Rev. B **94**, 144416 \(2016\)](#), [arXiv:1607.05110 \[cond-mat.str-el\]](#).
 - [21] N. Karthik and R. Narayanan, “Flavor and topological current correlators in parity-invariant three-dimensional QED,” [Phys. Rev. D **96**, 054509 \(2017\)](#).
 - [22] T. Sato, M. Hohenadler, and F. F. Assaad, “Dirac Fermions with Competing Orders: Non-Landau Transition with Emergent Symmetry,” [Phys. Rev. Lett. **119**, 197203 \(2017\)](#).
 - [23] G. J. Sreejith, S. Powell, and A. Nahum, “Emergent $SO(5)$ symmetry at the columnar ordering transition in the classical cubic dimer model,” (2018), [arXiv:1803.11218 \[cond-mat.stat-mech\]](#).
 - [24] F. F. Assaad and T. Grover, “Simple Fermionic Model of Deconfined Phases and Phase Transitions,” [Phys. Rev. X **6**, 041049 \(2016\)](#).
 - [25] S. Gazit, M. Randeria, and A. Vishwanath, “Emergent Dirac fermions and broken symmetries in confined and deconfined phases of Z_2 gauge theories,” [Nature Physics **13**, 484 \(2017\)](#), [arXiv:1607.03892 \[cond-mat.str-el\]](#).
 - [26] R. Nandkishore, M. A. Metlitski, and T. Senthil, “Orthogonal metals: The simplest non-Fermi liquids,” [Phys. Rev. B **86**, 045128 \(2012\)](#).
 - [27] S. Zhang, “Pseudospin symmetry and new collective modes of the Hubbard model,” [Phys. Rev. Lett. **65**, 120 \(1990\)](#).
 - [28] A. Auerbach, [Interacting electrons and quantum magnetism](#) (Springer Science & Business Media, 2012).
 - [29] J. B. Kogut, “An introduction to lattice gauge theory and spin systems,” [Rev. Mod. Phys. **51**, 659 \(1979\)](#).
 - [30] I. Affleck and J. B. Marston, “Large- n limit of the Heisenberg-Hubbard model: Implications for high- T_c superconductors,” [Phys. Rev. B **37**, 3774 \(1988\)](#).
 - [31] A. Kitaev, “Fault-tolerant quantum computation by anyons,” [Annals of Physics **303**, 2 \(2003\)](#).
 - [32] X.-G. Wen, “Quantum orders and symmetric spin liquids,” [Phys. Rev. B **65**, 165113 \(2002\)](#).
 - [33] I. F. Herbut, V. Juričić, and O. Vafek, “Relativistic Mott criticality in graphene,” [Phys. Rev. B **80**,](#)

075432 (2009).

- [34] F. F. Assaad and I. F. Herbut, “Pinning the Order: The Nature of Quantum Criticality in the Hubbard Model on Honeycomb Lattice,” [Phys. Rev. X **3**, 031010 \(2013\)](#).
- [35] F. Parisen Toldin, M. Hohenadler, F. F. Assaad, and I. F. Herbut, “Fermionic quantum criticality in honeycomb and π -flux Hubbard models: Finite-size scaling of renormalization-group-invariant observables from quantum Monte Carlo,” [Phys. Rev. B **91**, 165108 \(2015\)](#).
- [36] Y. Otsuka, S. Yunoki, and S. Sorella, “Universal Quantum Criticality in the Metal-Insulator Transition of Two-Dimensional Interacting Dirac Electrons,” [Phys. Rev. X **6**, 011029 \(2016\)](#).
- [37] S. Sachdev and T. Morinari, “Strongly coupled quantum criticality with a Fermi surface in two dimensions: Fractionalization of spin and charge collective modes,” [Phys. Rev. B **66**, 235117 \(2002\)](#), [cond-mat/0207167](#).
- [38] F. Assaad and H. Evertz, “World-line and Determinantal Quantum Monte Carlo Methods for Spins, Phonons and Electrons,” in [Computational Many-Particle Physics](#), edited by H. Fehske, R. Schneider, and A. Weiße (Springer Berlin Heidelberg, Berlin, Heidelberg, 2008) pp. 277–356.
- [39] M. Bercx, F. Goth, J. S. Hofmann, and F. F. Assaad, “The ALF (Algorithms for Lattice Fermions) project release 1.0. Documentation for the auxiliary field quantum Monte Carlo code,” [SciPost Phys. **3**, 013 \(2017\)](#).
- [40] S. Pujari, T. C. Lang, G. Murthy, and R. K. Kaul, “Interaction-Induced Dirac Fermions from Quadratic Band Touching in Bilayer Graphene,” [Phys. Rev. Lett. **117**, 086404 \(2016\)](#).
- [41] A. M. Polyakov, “Thermal Properties of Gauge Fields and Quark Liberation,” [Phys. Lett. **72B**, 477 \(1978\)](#).
- [42] S. V. Isakov, M. B. Hastings, and R. G. Melko, “Topological entanglement entropy of a Bose-Hubbard spin liquid,” [Nature Physics **7**, 772 \(2011\)](#), [arXiv:1102.1721 \[cond-mat.str-el\]](#).
- [43] T. Grover, Y. Zhang, and A. Vishwanath, “Entanglement entropy as a portal to the physics of quantum spin liquids,” [New Journal of Physics **15**, 025002 \(2013\)](#).
- [44] K. Fredenhagen and M. Marcu, “Confinement criterion for QCD with dynamical quarks,” [Phys. Rev. Lett. **56**, 223 \(1986\)](#).
- [45] K. Gregor, D. A. Huse, R. Moessner, and S. L. Sondhi, “Diagnosing Deconfinement and Topological Order,” [New J. Phys. **13**, 025009 \(2011\)](#), [arXiv:1011.4187 \[cond-mat.str-el\]](#).
- [46] S. Sachdev, “Topological order and Fermi surface reconstruction,” [ArXiv e-prints \(2018\)](#), [arXiv:1801.01125 \[cond-mat.str-el\]](#).
- [47] T. Senthil, L. Balents, S. Sachdev, A. Vishwanath, and M. P. A. Fisher, “Quantum criticality beyond the Landau-Ginzburg-Wilson paradigm,” [Phys. Rev. B **70**, 144407 \(2004\)](#), [cond-mat/0312617](#).
- [48] E. Fradkin and S. H. Shenker, “Phase diagrams of lattice gauge theories with Higgs fields,” [Phys. Rev. D **19**, 3682 \(1979\)](#).

- [49] S. Sachdev and D. Chowdhury, “The novel metallic states of the cuprates: Fermi liquids with topological order and strange metals,” [Progress of Theoretical and Experimental Physics](#) **2016**, 12C102 (2016), [arXiv:1605.03579 \[cond-mat.str-el\]](#).
- [50] S. Chatterjee, S. Sachdev, and M. Scheurer, “Intertwining topological order and broken symmetry in a theory of fluctuating spin density waves,” [Phys. Rev. Lett.](#) **119**, 227002 (2017), [arXiv:1705.06289 \[cond-mat.str-el\]](#).
- [51] S. Sachdev, M. A. Metlitski, Y. Qi, and C. Xu, “Fluctuating spin density waves in metals,” [Phys. Rev. B](#) **80**, 155129 (2009), [arXiv:0907.3732 \[cond-mat.str-el\]](#).
- [52] P. A. Lee, N. Nagaosa, and X.-G. Wen, “Doping a Mott insulator: Physics of high-temperature superconductivity,” [Rev. Mod. Phys.](#) **78**, 17 (2006), [cond-mat/0410445](#).
- [53] C. Xu and S. Sachdev, “Majorana Liquids: The Complete Fractionalization of the Electron,” [Phys. Rev. Lett.](#) **105**, 057201 (2010), [arXiv:1004.5431 \[cond-mat.str-el\]](#).
- [54] A. Thomson and S. Sachdev, “Fermionic Spinon Theory of Square Lattice Spin Liquids near the Néel State,” [Phys. Rev. X](#) **8**, 011012 (2018), [arXiv:1708.04626 \[cond-mat.str-el\]](#).
- [55] N. Karthik and R. Narayanan, “Scale-invariance and scale-breaking in parity-invariant three-dimensional QCD,” [Phys. Rev. D](#) **97**, 054510 (2018), [arXiv:1801.02637 \[hep-th\]](#).
- [56] Strictly speaking, the simulated QCD₃ at $N_f = 2$ does not have the full $SO(5)$ symmetry on the lattice scale, because the full symmetry is anomalous. In principle, there is a more exotic scenario[18], in which the QCD theory with full $SO(5)$ symmetry flows to the continuous Neel to VBS transition (the deconfined quantum critical point), and chiral symmetry breaking happens only when the full $SO(5)$ is explicitly broken (for example to $SO(3) \times SO(2)$). Our theory holds even if this scenario is correct, since the full $SO(5)$ is already broken in our microscopic model.
- [57] E. Huffman, “Monte Carlo methods in continuous time for lattice Hamiltonians,” [Proceedings, 34th International Symposium on Lattice Field Theory](#), (2016), [arXiv:1611.01680 \[hep-lat\]](#).
- [58] E. Huffman and S. Chandrasekharan, “Fermion bag approach to Hamiltonian lattice field theories in continuous time,” [Phys. Rev. D](#) **96**, 114502 (2017).
- [59] N. Karthik and R. Narayanan, “Scale invariance of parity-invariant three-dimensional QED,” [Phys. Rev. D](#) **94**, 065026 (2016), [arXiv:1606.04109 \[hep-th\]](#).
- [60] J. Alicea, “Monopole quantum numbers in the staggered flux spin liquid,” [Phys. Rev. B](#) **78**, 035126 (2008), [arXiv:0804.0786 \[cond-mat.str-el\]](#).
- [61] V. Borokhov, A. Kapustin, and X. Wu, “Topological Disorder Operators in Three-Dimensional Conformal Field Theory,” [Journal of High Energy Physics](#) **11**, 049 (2002), [hep-th/0206054](#).
- [62] E. Dyer, M. Mezei, and S. S. Pufu, “Monopole Taxonomy in Three-Dimensional Conformal Field Theories,” [ArXiv e-prints](#) (2013), [arXiv:1309.1160 \[hep-th\]](#).

- [63] J. Manuel Carmona, A. Pelissetto, and E. Vicari, “ N -component Ginzburg-Landau Hamiltonian with cubic anisotropy: A six-loop study,” [Phys. Rev. B **61**, 15136 \(2000\)](#).